4.6 Characterization and properties of the cycles

In the previous chapters, the synthesis and GPC separation of the cyclic products was described. For the key precursor molecules, comments on characterization and purity were given, and exemplary ^{1}H-NMR spectra were shown. The characterization of the macrocycles has not been described yet, but is completely comprised in this chapter, together with some investigations into the cycles' properties. The main reason for this is that specific problems are connected with the characterization of the macrocycles, which can be discussed in a comparative manner here.

All cyclization precursors are fully characterized, which includes ^{1}H/^{13}C-NMR, MS and correct EA. The macrocycles were separated by preparative GPC and the purified compounds showed monomodal traces (some examples were shown in previous chapters). The cycles were analyzed by MS and NMR to different extents, which is discussed in the following. The main problems arise from difficulties to dissolve the substances completely; this aspect is discussed first. Studies are finally accomplished by X-ray and STM measurements for some macrocycles. The higher mass cyclic oligomers which were separated are specifically problematic to be analyzed properly and are therefore described in an own chapter.

4.6.1 Solubility

All ring precursors are well soluble in common solvents like $CHCl_3$, THF or toluene. When these flexible compounds are transferred into more rigid species by cyclization, solubility can be expected to show a tendency to decrease. Principally, the macrocycles can be viewed as a collection of aromatic rings held in a rigid framework, thus amplifying the effects by π-π interactions. The cycles should therefore be best soluble in aromatic solvents like benzene or toluene.[143] This, however, was not found to be the case when handling the cycles. Quantitative numbers for the solubility of a selection of the macrocycles were therefore determined in chloroform, with an additional measurement for **95b** in toluene (Table 4).

Concentrated solutions of the compounds were gained by shaking an excess of material in $CHCl_3$ overnight. After filtration, defined volumes (~ 0.5 – 1 ml for the less soluble, ~ 0.01 ml for the better soluble cycles) were transferred via an Eppendorf pipette to a probe glass, the solvent evaporated, the residue dried in high vacuum and weighed. This was done twice for each entry; the numbers show a considerable deviation, and averages are approximate values. This is due to the practical problems measuring the solubility of

compounds in relatively small quantities. For the poorly soluble cycles, very small amounts had to be weighed. For the well soluble cycles, the solutions became viscous and extremely difficult to handle, as they tended to dry and precipitate.

Tab. 4 Solubilities of macrocycles in $CHCl_3$ (except [a]: toluene). [b]: Values were measured from an unsaturated solution.

Cycle	Measured solubility (mg/ml)	Average (mg/ml)	Average (mol/l)
88	2.5 2.6	≈ 3	$\approx 2\times10^{-3}$
95a	388 247	≈ 300	$\approx 2\times10^{-1}$
95b	4.4 4.4	≈ 4	$\approx 3\times10^{-3}$
95b[a]	7.3 3.4	≈ 5	$\approx 3\times10^{-3}$
95d	371 378	≈ 350	$\approx 2\times10^{-1}$
106	> 325[b)] > 225[b)]	> 300[b]	$> 1.0\times10^{-1}$[b]
111	7.0 4.9	≈ 6	$\approx 4\times10^{-3}$

Despite the large errors, the values show clear tendencies. The most stunning observation is surely, that the cycles are either poorly (**88**, **95b**, **111**), or quite well soluble (**95a**, **95d**, **106**). To give a better understanding of these values, compare data of well-known substances:[144] naphthalin ($CHCl_3$, 21°C): 200 mg/ml, 1.6 mol/l;[145] theobromine ($CHCl_3$, 20°C): 0.25 mg/ml, 1.4×10^{-3} mol/l.[146]

A change in solvent, from $CHCl_3$ to toluene (**95b**), has practically no effect. The number and position of side chains obviously plays a role, as expected. A cycle carrying a terphenyl unit with one exocyclic hexyloxy side chain (**95b**) is much less soluble than the same cycle, but with a terphenyl unit with four hexyl side chains (**95d**). If one compares 46-membered **95a** and its 58-membered analogue **106**, which has the same number of side chains, but two more phenylacetylene units (ratio ring members/side chains 9.2 for **95a**, 11.6 for **106**), one practically sees no difference in solubility, however.

The terpyridine units generally lead to a decrease in solubility; cycles with two terpyridine units are generally poorly soluble, and this is not due to a smaller number of side

chains only. For example, for poorly soluble **88** (with 2 terpyridine units), the ratio ring members/side chains is 11.5 and the ratio aromatics / side chains 2.5, while the well soluble **106** (with one terpyridine unit) has nearly the same values of 11.6 and 2.4, resp. An influence of the higher symmetry of the cycles with 2 terpys (D_{2h}) versus those with one terpy (C_{2v}) cannot be excluded, however.

The perhaps most interesting observation here results from the comparison of cycles **95a** and **95b**. The only difference between these cycles is that **95b** carries 4 hexoxy side chains at its corners, while **95a** has 4 hexoxymethyl side chains at the same positions. Even if one expects a better solubility in the case of the benzyl ether – the oxygen is separated from the aromatic, while for the phenol ether, the aromatic-oxygen bond has partially double bond character due to mesomeric effects – the large effect is astonishing. Other than **88** and **111**, which are nearly insoluble in common solvents even under heating, **95b** dissolves easily in warm THF or benzene but precipitates, however, under cooling.

4.6.2 Mass spectrometry

To analyze the precursor molecules described in this work, the electron beam ionization (EI) method was found to give the most reliable results. As the substance is evaporated thermally from the bulk and ionized in the gas phase, only signals of the molecule ion and fragmentation ions thereof are recorded. Larger molecules, which are less easily evaporated, like some of the extended terpyridines and the macrocycles, were analyzed by FAB(+)-measurements. Here, the ions are brought into the gas phase from a matrix, and not only fragmentations, but also adduct formations and signals due to the matrix material are observed. As a typical example, the FAB(+) spectrum of **110a** (Fig. 19) shows not only a high baseline, which makes statements about the purity of the substance difficult, but also a number of signals at m/z values higher than $[M]^+$. These can be assigned to adducts of M and characteristic fragments thereof (for these characteristic fragmentations, ref. the MS data for practically all the substances with hexyl side chains given in the Experimental Part).

MALDI-TOF is a much milder MS method for large molecules.[147] Generally, no fragmentations occur. In contrast to the FAB spectrum, the MALDI-TOF spectrum for **110a** indeed shows a much smoother baseline (Fig. 20). However, a number of additional peaks are also detected here, which can be assigned to fragmentation and adduct formation. Especially the latter, i.e., the observation of signals at m/z values higher than [M+H] or [M+Na/K], unfortunately hampers statements about the purity of the compounds, as it cannot be clearly proved that these signals are really adducts and not in fact fragments of higher mass

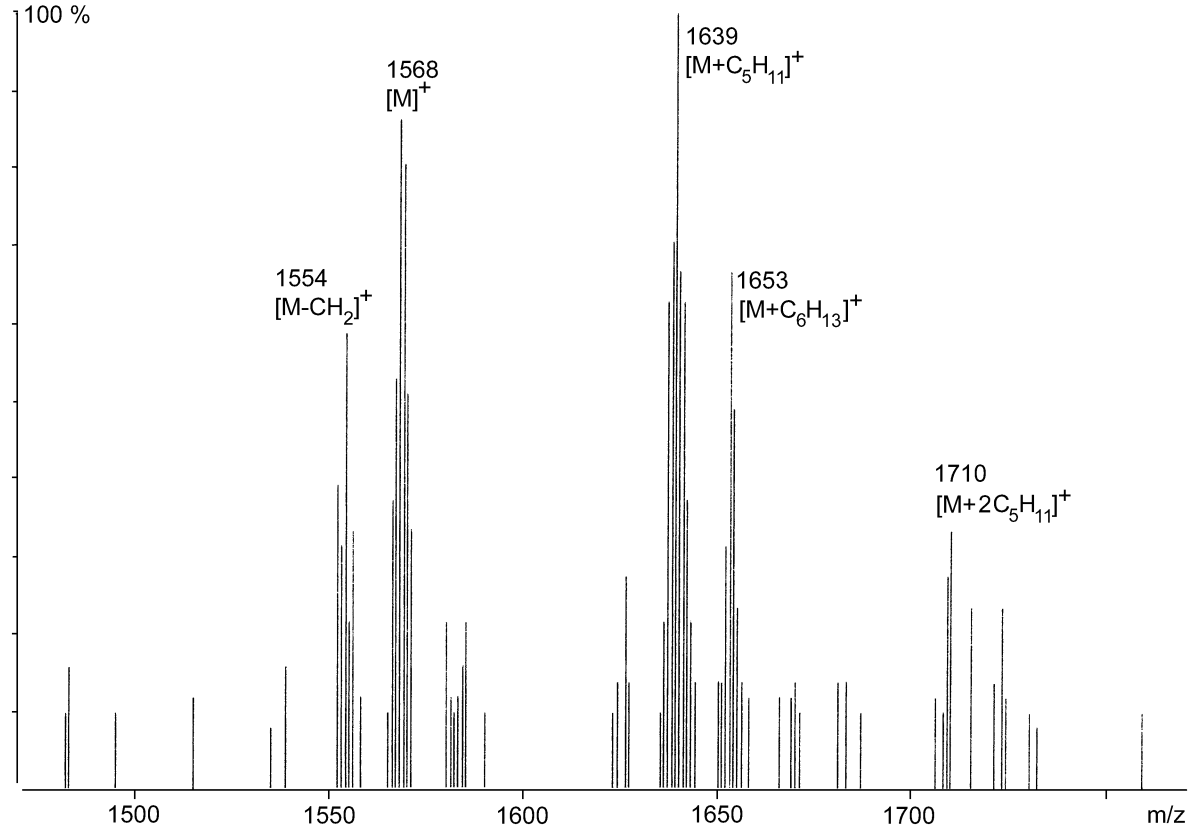

*Fig. 19. FAB(+)-MS spectrum (excerpt) of macrocycle **110a**.*

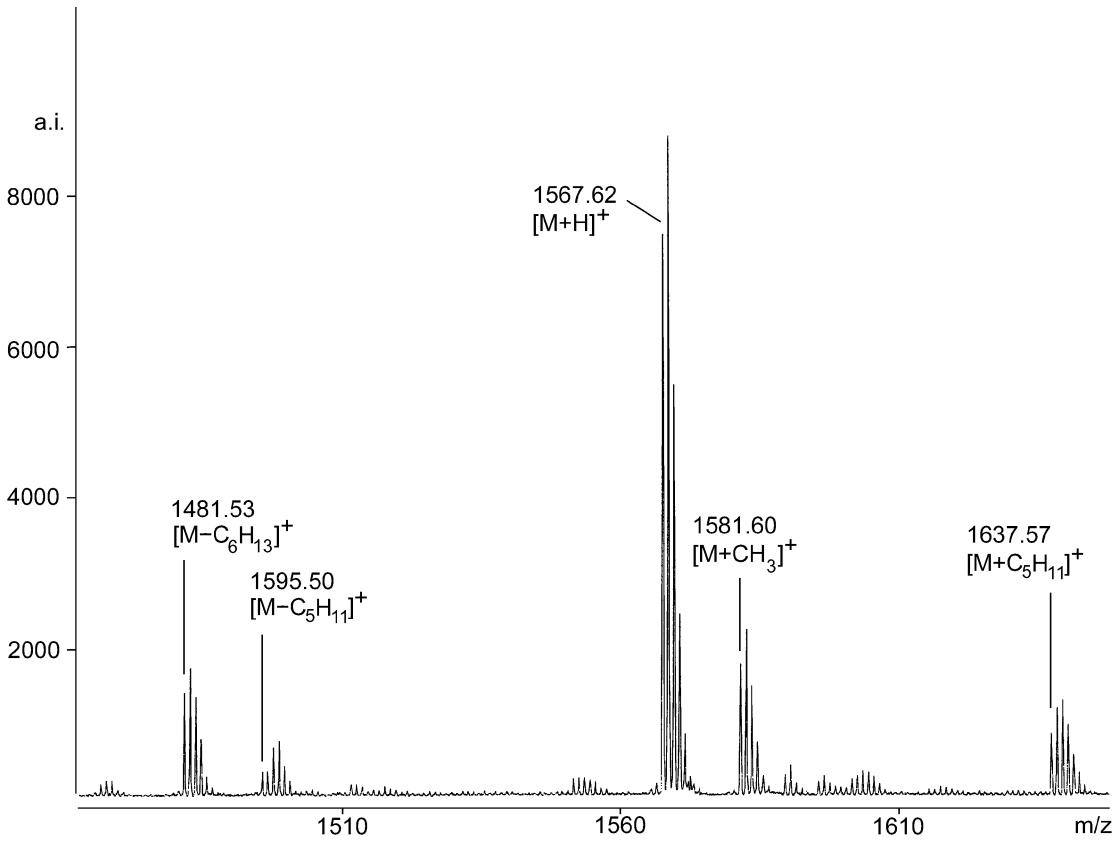

*Fig. 20. MALDI-TOF MS spectrum (reflector mode, excerpt) of macrocycle **110a**.*

impurities. The fragmentation and formation of clusters between matrix and analyte has also been observed by Höger for his macrocycles.[148] He detected clusters of up to 8 macrocycles in the spectrogram. This, however, has not been found here. MALDI spectra were recorded for **88**, **95a**, **95c**, **106**, **110a-c** and **111** and appear comparable to the one shown in Fig. 20. For **88**, **95c** and **110c**, peaks with lower intensity appear at higher m/z values which cannot be assigned (also not to open-chain dimers expected from incomplete reaction) and may either represent adducts or impurities. For cycles **95b** and **95d**, only FAB(+) measurements were recorded; the structure of these compounds, however, is proven by X-ray diffraction.

For oxidative alkynyl-alkynyl cyclization reactions, the mass difference between the macrocycles and their open-chain precursors is only 2 Da. This small difference, however, is clearly detected in MALDI measurements and allowed Henze to analyze the open-chain precursor which he isolated as main product in a Glaser cyclization;[30] this assignment was further proven by NMR. From modified reaction conditions, he could get the desired cycle. Even if this was not separated, its characteristic peak was detected in MALDI. The MALDI-TOF spectrum of **111** clearly shows the protonated macrocycle as main peak; no signal which could be attributed to the open-chain precursor is detectable.

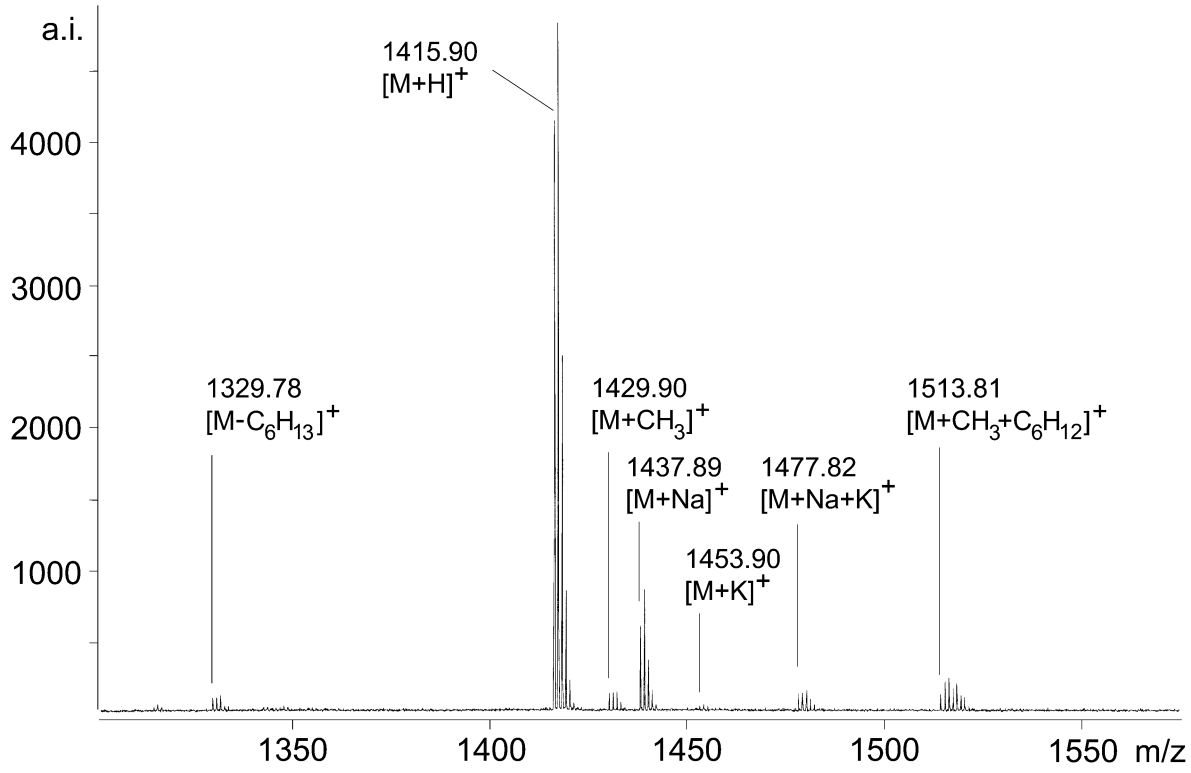

*Fig. 21. MALDI-TOF MS spectrum (reflector mode, excerpt) of macrocycle **111**.*

4.6.3 NMR measurements

Besides the requirements on NMR spectra which are common for all organic substances - minimal impurities and signals consistent with the proposed constitution - additional information for specific classes of substances are also accessible with this method, e.g., about their conformation. In the case of the macrocycles, it is their cyclic nature itself which represents the main issue: how to positively prove as far as possible that the compound is cyclic and not linear?

The main argument bases on the fact that a reduced number of signals appears in the NMR due to the higher symmetry of the cyclic versus the linear analogue of a similar molar mass. This, however, may be difficult to verify for cycles like **95b** with only one terpyridine unit. Their symmetry is only C_{2v}, and a high number of overlaying signals can be observed in the aromatic region.

Another aspect is the complete disappearance of signals due to the coupling functionalities. This may be difficult to observe for the halo-functions. Signals of X-C groups in the ^{13}C may be very weak, and the neighbored H atoms may not be separated clearly enough in the ^{1}H spectrum. The proton of the free acetylene unit, however, shows a very characteristic, sharp singlet at δ = 3.3 ppm, which is separated from all other signals and can easily be detected.

Therefore, all synthesized macrocycles in the optimum case should have been investigated as far as possible by NMR spectroscopy. The following problems, however, were encountered:

- Some of the cycles were poorly soluble (ref. Chapter 4.6.1), and no ^{13}C spectra could be recorded.
- In all cases, which were investigated by 2-D NMR measurements, a strong dependency of the chemical shifts on concentration and temperature was observed. This effect has been described for a number of phenylacetylene macrocycles and was attributed to aggregation.[7,16,17,115,149]
- For some cycles, signals were extremely broad, probably also an effect of aggregation.

All cycles with one terpyridine unit (**95a-d**, **106**) were analyzed by ^{1}H-, ^{13}C-, COSY- and HETCOR-NMR measurements (Fig. 22). Thus it was possible to assign all proton and carbon signals, even if a differentiation of similar signals was sometimes not possible. It was possible to assign the signals for the terpyridine unit, the terphenyl unit and the aromatic corner units separately from each other. It was in no case possible, however, to find cross signals which could clarify the connectivity of these units via the acetylene bridges,

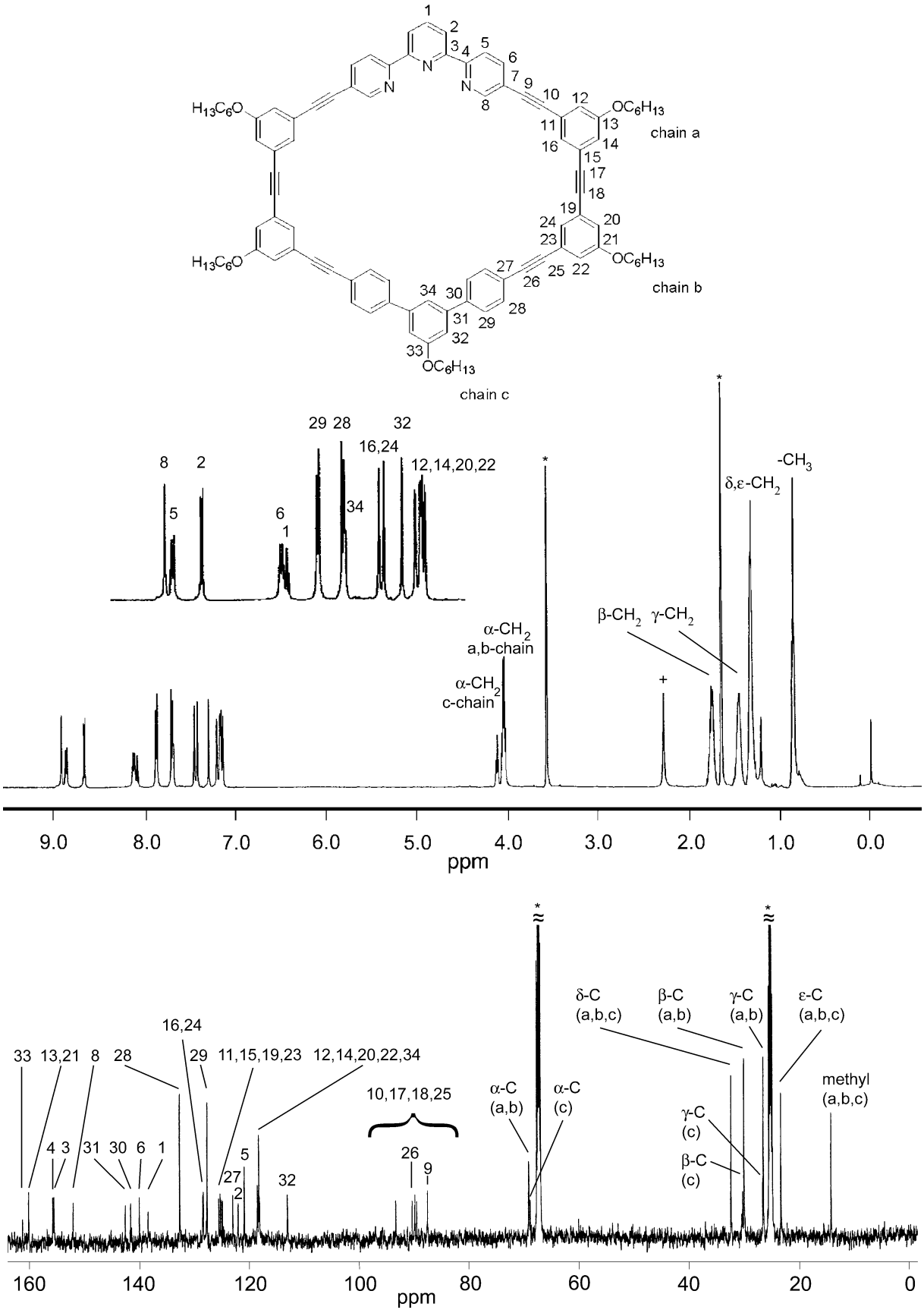

*Fig. 22. [1]H-NMR spectrum (500 MHz, d^8-THF, 320 K) of macrocycle **95b** (top); [13]C-NMR spectrum (125.8 MHz, d^8-THF, 320 K) of macrocycle **95b** (bottom); * = d^8-THF; + = H_2O.*

for example, the ^4J coupling between 6-H and 10-C in Fig. 22. Thus, it was possible to assign all signals belonging to each of the corner aromatics but not to decide which aromatic was which. Accordingly, it was not possible to decide which side of the aromatic was connected to which of the two different acetylene bridges. Except for **95b**, which had to be measured in d^8-THF at elevated temperature, the before mentioned macrocycles were measured in $CHCl_3$ at ambient temperature.

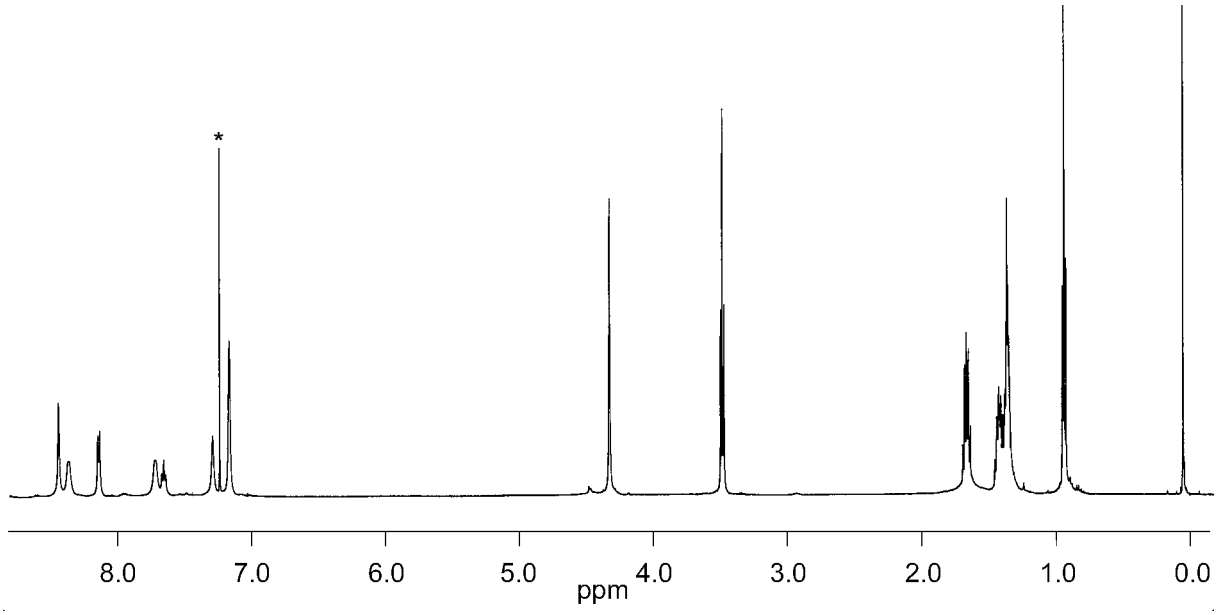

*Fig. 23. ^{1}H-NMR spectrum (500 MHz, $CDCl_3$) of macrocycle **111**; * = $CDCl_3$.*

For macrocycles **88** and **111** with two terpyridines, no ^{13}C spectra could be recorded due to their low solubility. The reduced set of signals in their ^1H spectra proves nevertheless their cyclic nature (Fig. 23). No additional signals are observed which may be due to the unsymmetry of open-chain compounds, and especially, the characteristic peak of an acetylenic proton at δ = 3.3 ppm is not observed; **111** was cyclized via oxidative acetylene-acetylene coupling.

The 58-membered macrocycles with two terpyridine units and only 4 side chains, **110a** and **110b**, showed extremely broad signals in the ^1H-NMR. In the very first spectrum of **110a**, which was measured in $CDCl_3$ (Fig. 24 bottom), practically no signals were detected which could be assigned to the terpyridine unit (8.0-9.0 ppm). Successive dilution led to the appearance of signals in this region, which were still very broad (Fig. 24 middle). In another measurement, to a solution of **110a** in $CDCl_3$, d-TFA was successively added. The solubility of **110a** improved with decreasing pH, and for approx. $CDCl_3$/d-TFA 1:1, a spectrum was obtained which showed at least some resolution (Fig. 24 top).

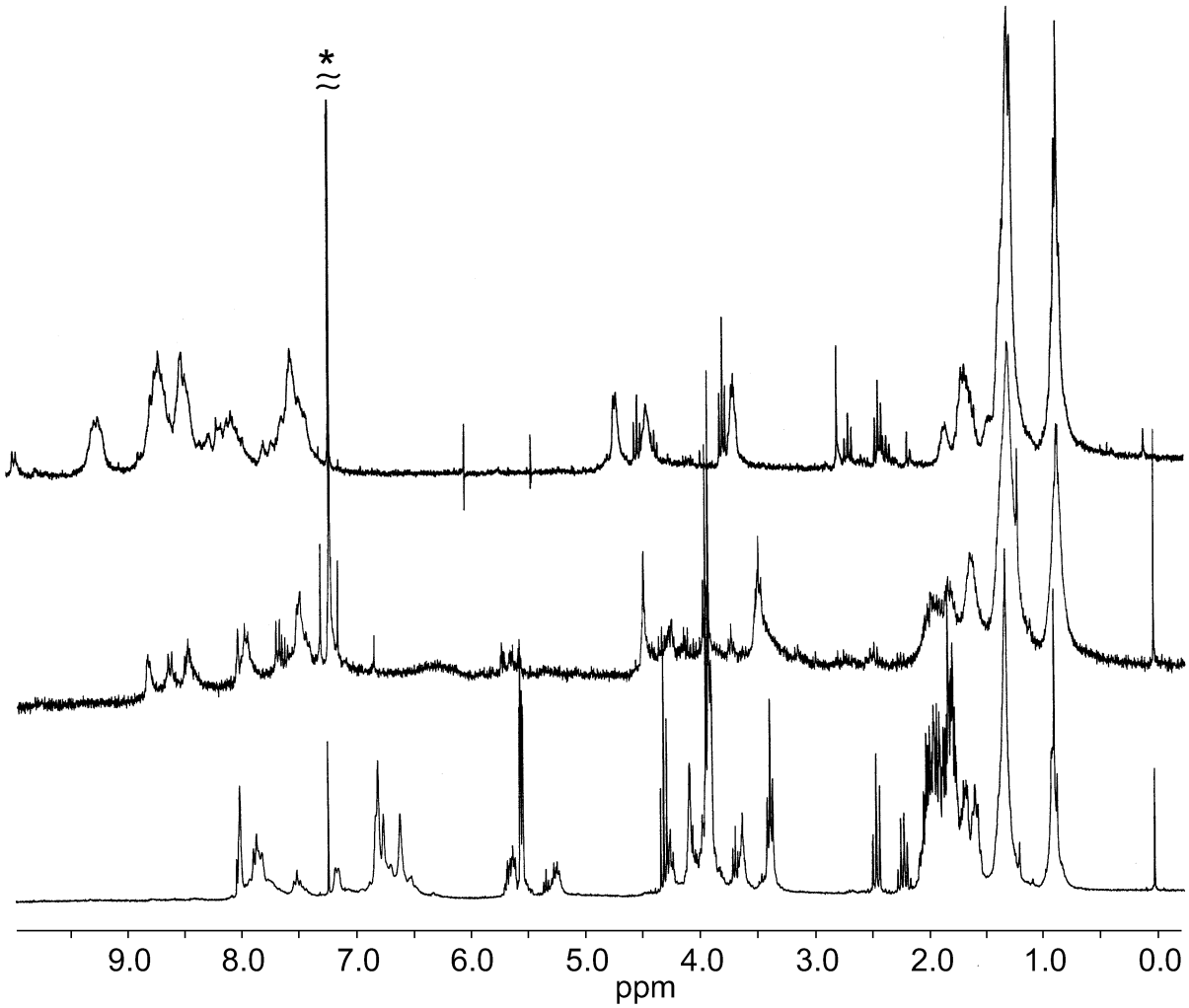

*Fig. 24. ^{1}H-NMR spectra (270 MHz, $CDCl_3$) of macrocycle **110a**. Bottom: At higher concentration; middle: at lower concentration; top: in $CDCl_3$/d-TFA 1:1; * = $CDCl_3$; d-TFA signal at 11.5 ppm cut.*

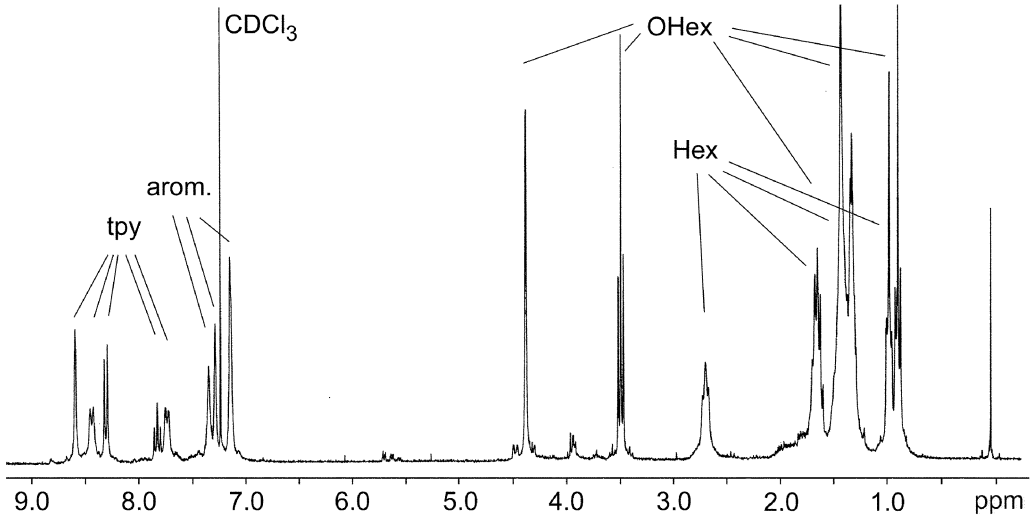

*Fig. 25. ^{1}H-NMR spectrum (270 MHz, $CDCl_3$,) of macrocycle **110c**.*

Macrocycle **110c** has the same backbone like **110a** but contains 4 more side chains. For entropic reasons, a lower tendency to form aggregates can be expected. The ^{1}H-spectrum of **110c** indeed shows a set of defined signals which could be assigned to the expected structure (Fig. 25). The signals at appr. δ = 6.5 ppm and δ = 1.8 ppm belong to the characteristic impurities from GPC separation.[185] However, after a few days the substance was only poorly soluble in $CDCl_3$, and the ^{1}H-NMR spectrum obtained showed a significant broadening of peaks as well as additional peaks. By adding d-TFA, most of the precipitate could be brought into solution again. Spectra with well resolved signals were obtained and allowed the characterization of **110c** by ^{1}H-, ^{13}C-, COSY- and HETCOR-NMR spectrometry. The ^{1}H-spectrum, however, seemed even less pure than that which was measured directly after GPC separation (Fig. 25). Probably this is not only due to impurities, but also to different protonated and unprotonated species.

4.6.4 X-ray analysis on single crystals[150]

Various attempts were made to grow crystals of the macrocycles by slow diffusion of a non-solvent (e.g., methanol) into a solution of the macrocycle (e.g., toluene). Interestingly, for none of the cycles with two terpyridine units or higher cyclic oligomers crystals were obtained but for all prepared cycles with only one terpyridine unit. All examined macrocycles crystallize with solvent molecules and therefore tend to disintegrate with loss of the included solvent molecules. The crystals were mounted out of saturated solutions at low temperature on the top of a glass fiber and the data collection was performed at low temperature as well. For **95a**, **95b** and **95d**, the crystals could be measured by X-ray diffraction and the structures dissolved. Also for the larger macrocycle **106**, crystals could be grown. During the sample preparation, however, they disintegrated even in an atmosphere of cold nitrogen. For **95c**, which is obtained as a mixture of diastereomers due to its THP side chains, the crystals were twinned and did not allow a structure elucidation by X-ray diffraction.

Macrocycle 95a

Crystals were obtained by slow diffusion of methanol into a solution in toluene. **95a** contains two molecules of toluene per formula unit and crystallizes in the triclinic space group P-1 with two molecules in the asymmetric unit (Figs. 26-29).

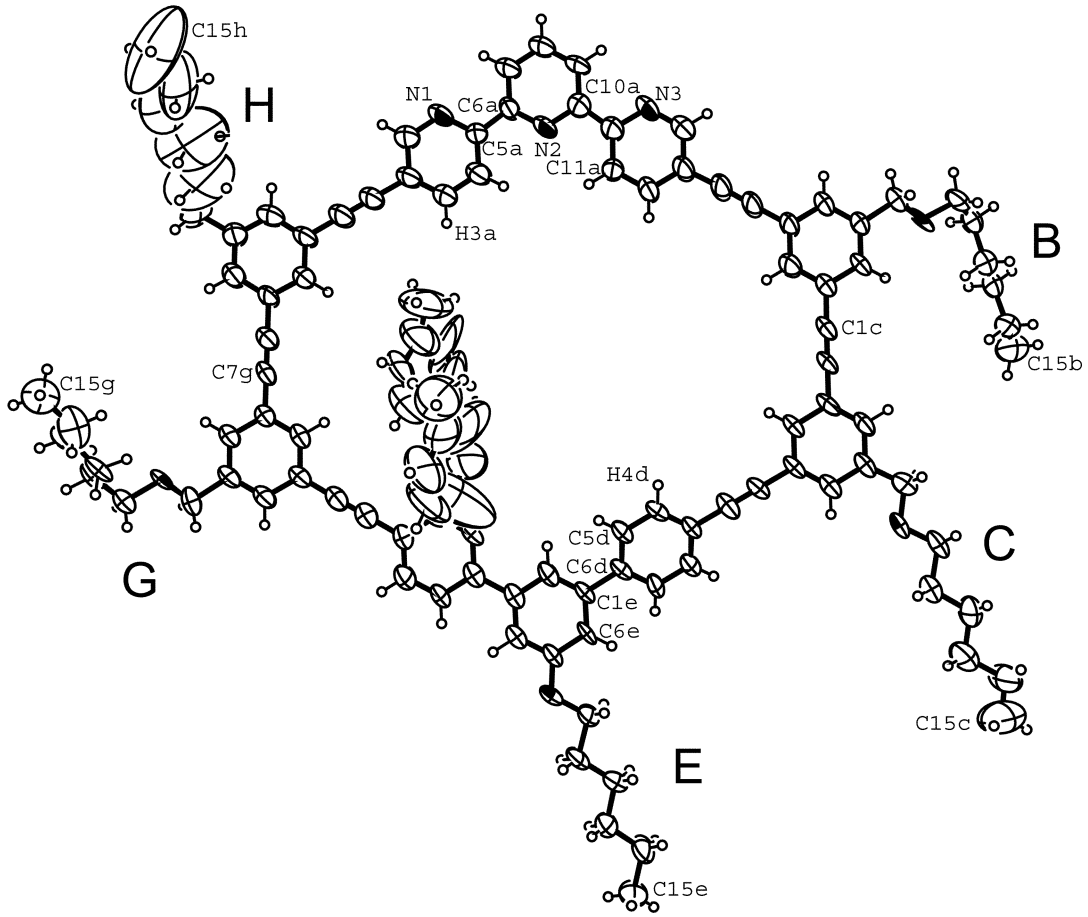

*Figure 26. ORTEP plot[151] of macrocycle **95a**, view perpendicular to the macrocycle, 50 % probability ellipsoids, with solvent molecules included in the crystal.*

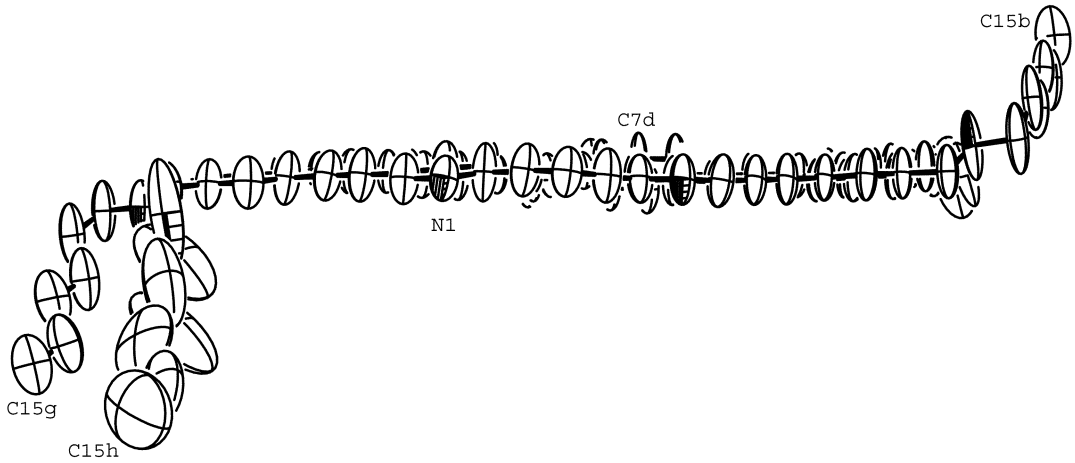

*Figure 27. ORTEP plot[151] of macrocycle **95a**, view parallel to the macrocycle, 50 % probability ellipsoids; H atoms and solvent molecules eliminated.*

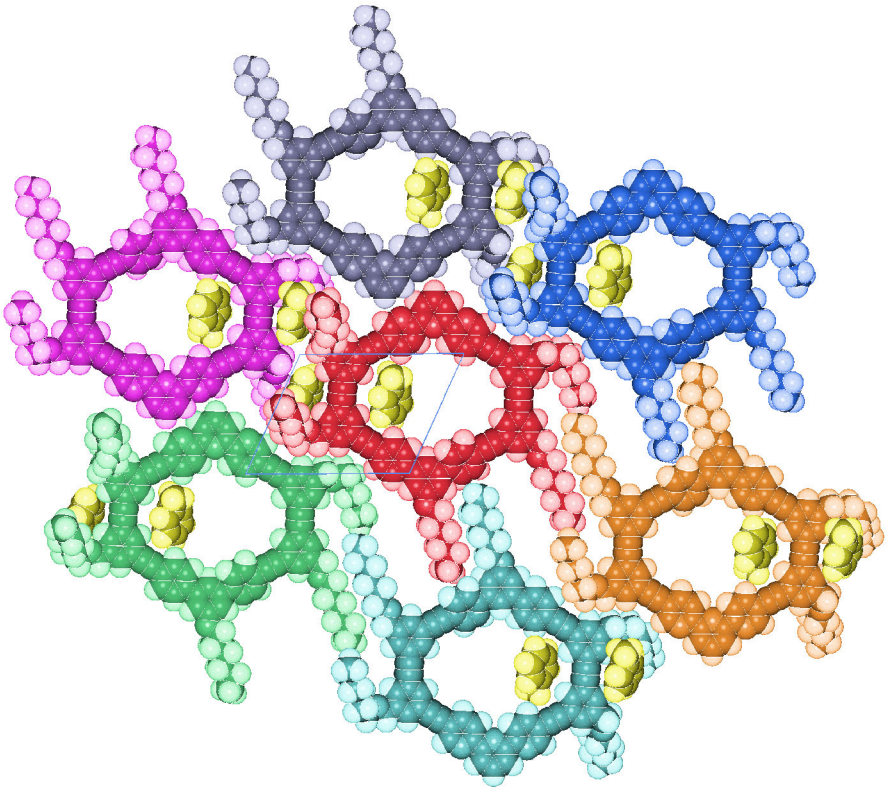

Figure 28. Space filling model (Schakal99)[153] *of one layer of* ***95a****, view along 0 -1 0, solvent molecules colored in yellow. Different colors were used to distinguish molecules generated by the following symmetry operations: x, y, z red; -1+x, 1+y, z green; 2-x, 2-y, 1-z violet; 3-x, 1-y, 1-z gray; 1+x, -1+y, z blue; -x, -2-y, -z orange; -1-x, -1-y, -z turquoise.*

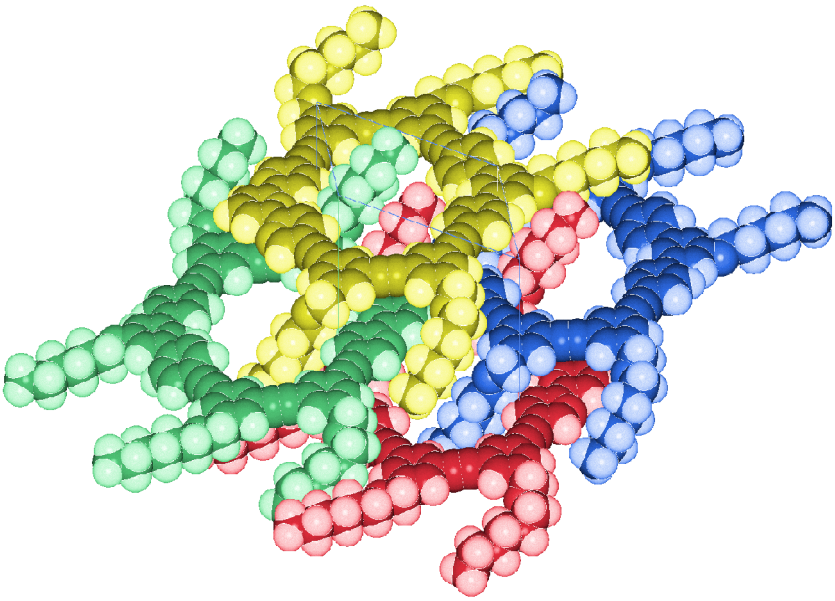

Figure 29. Space filling model (Schakal99)[153] *of the packing of* ***95a****, view roughly along 0 1 0, solvent molecules omitted for clarity. Different colors were used to distinguish molecules generated by the following symmetry operations: x, y, z red; 1-x, 1-y, 1-z yellow; -1+x, y, z green and 2-x, 1-y, 1-z blue.*

The individual cycles form almost planar sheets, but possess great positional freedom perpendicular to the plane sheet as expressed by the large thermal ellipsoids (Fig. 27). The aromatic ring h of the terphenyl unit, however, is tilted out of plane (C6e-C1e-C6d-C5d -149.6°, Fig. 26) As observed in most sterically unrestricted terpyridines,[121,152] the N-C-C-N torsion angles are close to 180° (N1-C5a-C6a-N2 166.8°, N2-C10a-C11a-N3 178.5°). The data does not allow an unambigous assignment of the nitrogens, which may be disordered. The largest distance across the hole inside the macrocycle, which is occupied by solvent molecules and side chains of neighbored molecules, is between the acetylenic carbon atoms (C1c-C7g 1.919 nm). The shortest inner diameter is C3a-C4d 1.200 nm.

Similar to what has been observed for other shape-persistent macrocycles, like Moore's phenylacetylenes[3] and Henze's recently published bipyridine containing macrocycles,[32,33] the cycles form a layered structure in the crystal. Figure 28 shows one layer of molecules in a view along the crystallographic c axis. Solvate molecules are colored in yellow for clarity. The molecules within the layer are in close contact at the terpyridine units. The two in plane side chains C and E of two adjacent rings are arranged anti parallel to each other. The methyl group of the hexyl chain E turns the benzene ring D out of the plane of the macrocycle. Further close contacts are visible at the starting point of chain B. The remaining side chains point above and below the backbone of the macrocycle linking together adjacent layers as can be seen in Figure 29. The side chains G and H are oriented almost perpendicular to the macrocycle's backbone. Chain H, which shows the largest disorder, penetrates the interior of a macrocycle of the next layer and reaches into the space between the sides of two adjacent macrocycles in the next but one layer; chain G shows opposite behavior.

Macrocycle 95b

Macrocycle **95b**, when dissolved in hot THF, benzene or toluene, crystallizes readily after cooling down. The X-ray analysis reported here was done with crystals grown from a benzene solution; a previous attempt to solve the structure for a crystal grown from THF failed, probably due to the high conformational freedom of the enclosed THF molecules.[154]

95b crystallizes in the triclinic space group P-1 with two molecules in the asymmetric unit and contains 3 molecules of benzene per formula unit. The individual cycles form almost planar sheets, but with less positional freedom than **95a** (Fig. 30). The rotation of one of the aromatic rings of the terphenyl unit out of plane (C4g-C5g-C1h-C6h 147.2°, Fig. 27), the N-C-C-N torsion angles (N1c-C1c-C5b-N1b 173.7°, N1b-C1b-C3a-N1a –175.6°), and the dimensions of the cycles' interior (C4l-C10l 1.992 nm, C4c-C5h 1.248 nm) are comparable to **95a**.

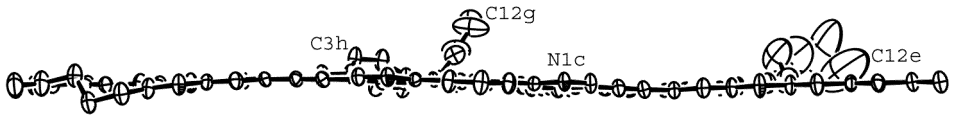

*Figure 30. ORTEP plot[151] of macrocycle **95b**, view parallel to the macrocycle, 50 % probability ellipsoids; H atoms and solvent molecules eliminated.*

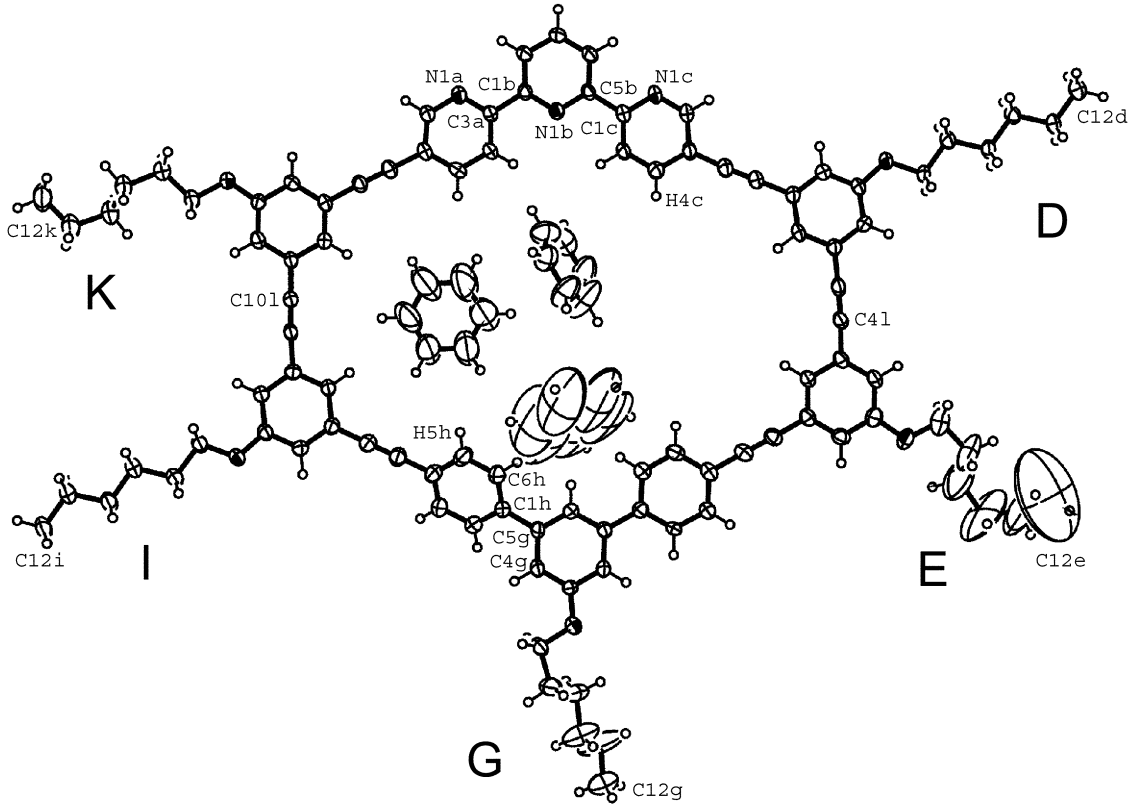

*Figure 31. ORTEP plot[151] of **95b**, view perpendicular to the macrocycle, 50 % probability ellipsoids, with solvent molecules included in the crystal.*

The packing, however, differs a lot from that of **95a**. Figure 32 presents a view along 0 1 1 on 7 adjacent molecules of **95b** within one layer. Again the molecules within the layer are in close contact at the terpyridine units and at four of the five hexyloxy side chains. The almost linear side chain D sticks in between the almost linear chain I and chain K, which on its opposite side is in close contact to a neighboring macrocycle. Chain K does not show the favorable all-trans conformation of extended alkanes, but is restricted by a neighbored benzene molecule. The chain G leans on one aromatic ring of a terphenyl unit of a

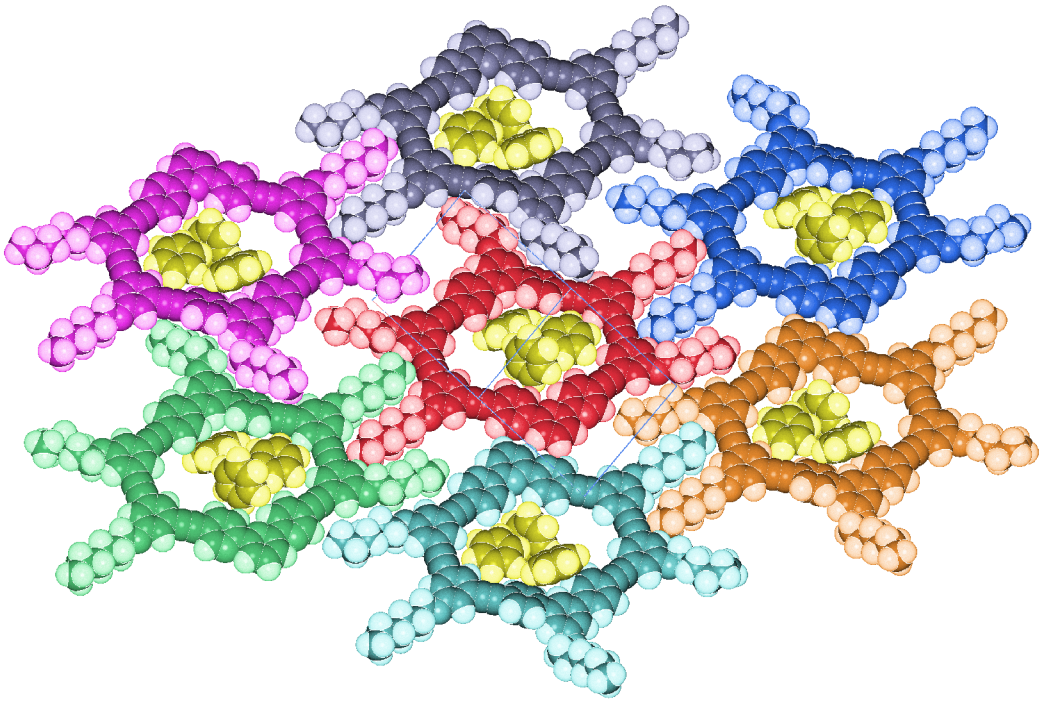

*Fig. 32. Space filling model of one layer (Schakal99[153]) of **95b**, solvent molecules are colored yellow. View along 0 -1 -1. Different colors were used to distinguish molecules generated by the following symmetry operations: x, y, z red; -2+x, 1+y, z green; -x, 2-y, -z violet; 2-x, 1-y, -z gray; 2+x, -1+y, z blue; 2-x, -1-y, 1-z orange; -x, -y, 1-z turquoise.*

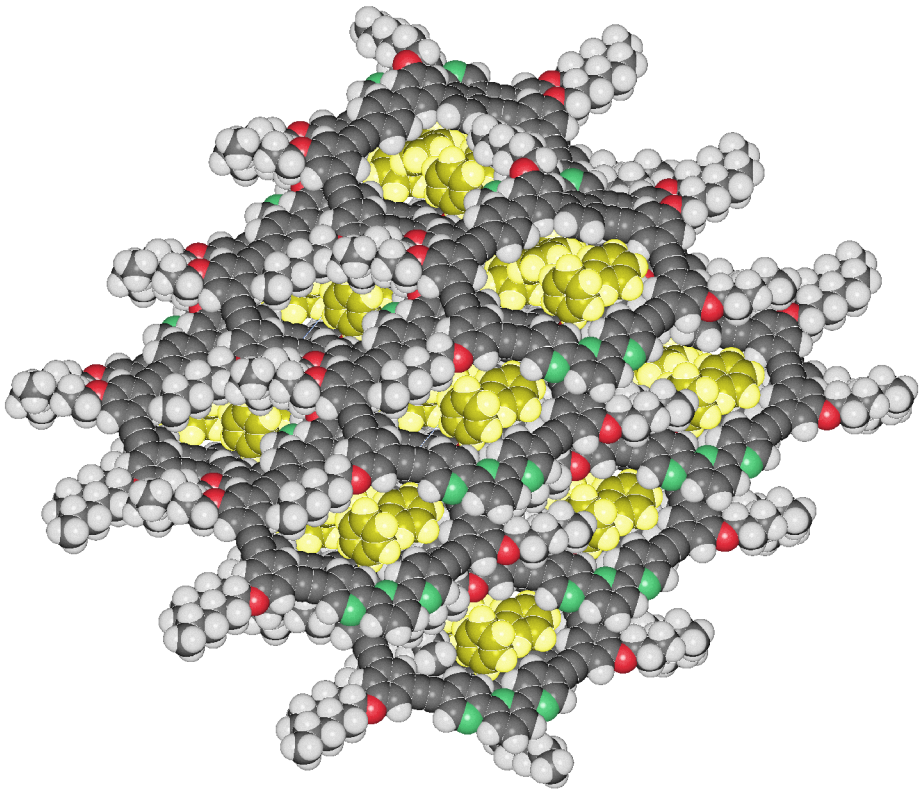

*Fig. 33. Space filling model of the packing (Schakal99)[153] of **95b**, solvent molecules are colored yellow. View along 0 -1 -1.*

neighboring macrocycle. This results in the abovementioned torsion of the aromatic ring H while all other aromatics are in plane with the cyclic backbone. The only side chain which has no closest contacts to neighboring molecules within the same layer is chain E which interestingly has very large thermal parameters and is near the solvate molecules with great positional freedom as can be seen from the ORTEP representation in Figure 31. All in all, the packing within one layer reminds one of interacting gear wheels. The remaining free volume is filled with side chains and solvate molecules interlocking adjacent layers. The sides of the cycles overlay in all directions, whereby subsequent layers are shifted against each other (Fig. 33). Removal of the solvent molecules would create channels almost along 0 1 1. However, these are not perpendicular to the plane of the molecules.

Macrocycle 95d

Crystals were obtained by slow diffusion of methanol into a solution in benzene. Also this macrocycle crystallizes in the triclinic space group P-1 with two molecules in the asymmetric unit and contains 3 molecules of benzene per formula unit (Fig. 34).

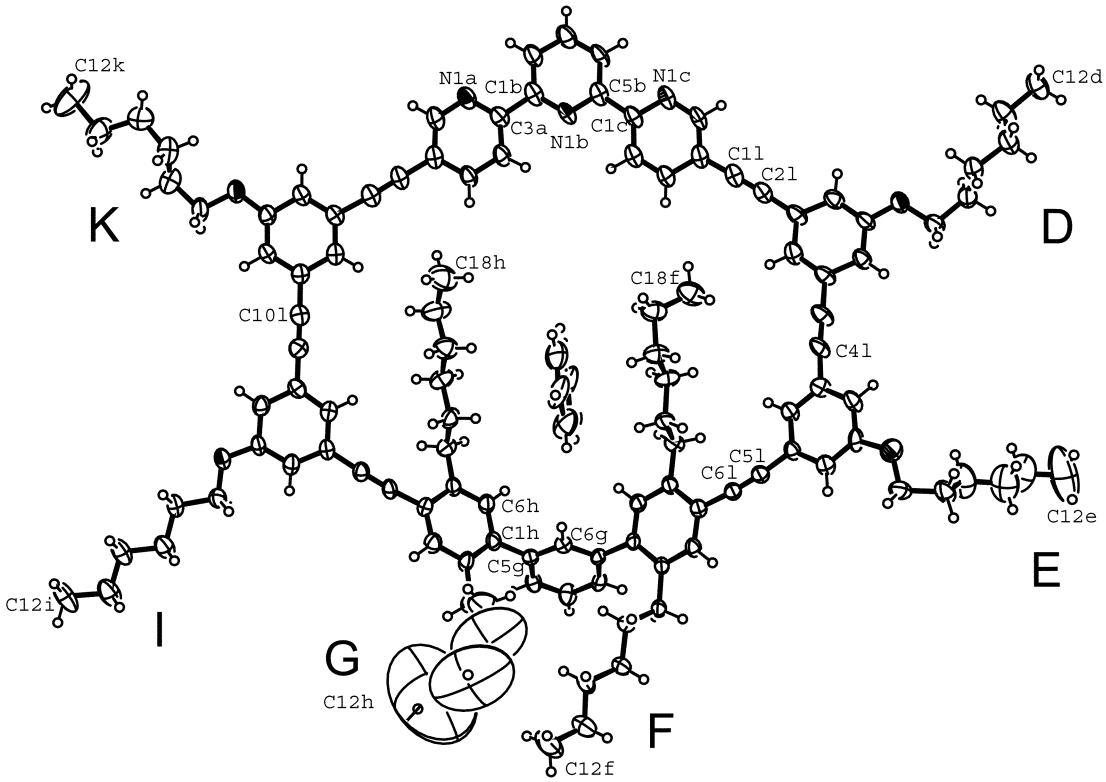

Figure 34. ORTEP plot[151] of *macrocycle* ***95d****, view perpendicular to the macrocycle, 50 % probability ellipsoids; two of the three solvent molecules per formula unit included in the crystal were eliminated.*

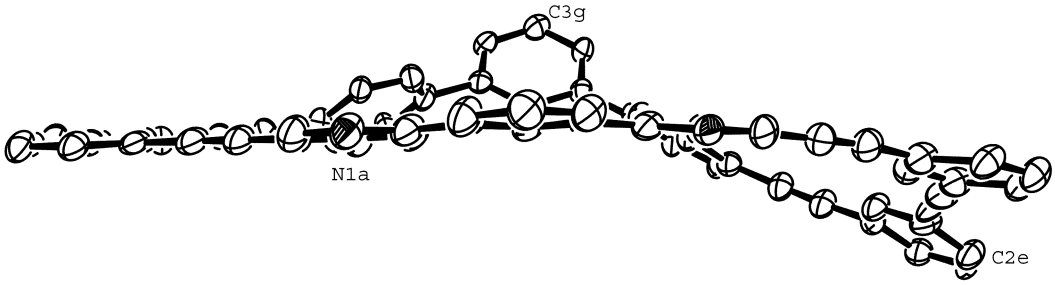

Figure 35. ORTEP plot[151] *of macrocycle* ***95d****, view parallel to the macrocycle, 50 % probability ellipsoids; H atoms, solvent molecules and side chains eliminated.*

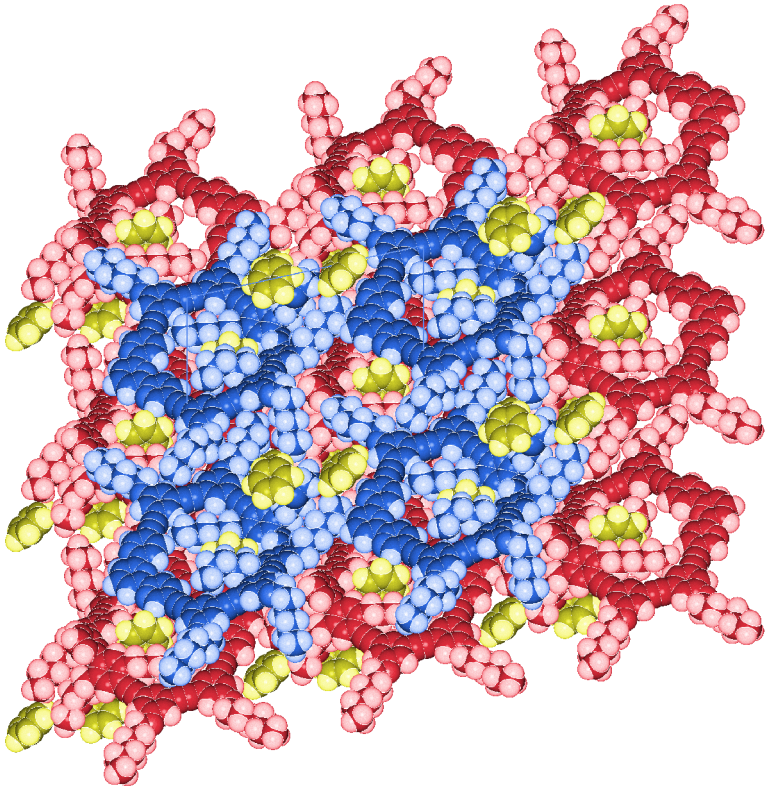

Figure 36. Space filling model (Schakal99)[153] *of two layers of* ***95d****, view along - 1 0 0, solvent molecules colored in yellow. Two different colors were used to clarify the layered structure, but do not imply that the molecules are crystallographically different.*

95d carries three more side chains than the cycles previously discussed, while having the same backbone size. The macrocycle, instead of forming planar sheets, is heavily distorted (C1l-C2l-C5l-C6l 25°, C6h-C1h-C5g-C6g 70°, Fig. 35). The inner diameters, however, are quite well in accordance with those above (C4l-C10l 1.840 nm, C4c-C5h 1.343 nm), and this

holds true also for the terpyridine conformation (N1a-C3a-C1b-N1b 176.2°, N1b-C5b-C1c-N1c –171.1°).

The packing follows a more simple AB layer pattern along the a axis. Furthermore, the packing of **95d** differs from the other cycles by the fact that there is overlap between the cycles only in direction of the b axis. This gives rise to formation of new layers along the b axis. The space between these layers is mainly filled with side chains, but also contains the only "true channels" in these structures, i.e., two neighboring channels which are throughout the crystal only filled with solvent molecules and not with side chains. The most highly disordered components of the structure share their parts with them: They are filled with the two benzene molecules, which lie roughly perpendicular to each other, and separated by outer side chain F. The inner F and H side chains stretch through the interior space of the cycle with one benzene molecule sandwiched between them. A K chain from a cycle of the next layer also reaches in. The remaining side chains pack into the space between the cycles.

4.6.5 STM-measurements on monolayers[155]

A great effort has been devoted in the last decade to understanding and controlling the physisorption of phenylene based rod-like and disk-like molecules into ordered nanostructures at the solution-highly ordered pyrolitic graphite (HOPG) interface.[156] These explorations have recently also been reported by means of STM focussing on Höger's phenylacetylene macrocycles[115], Bäuerle's thiophene[61,62] and Henze's bipyridine containing macrocycles.[31]

STM measurements were done for macrocycles **95d**, **110a** and **110c**. Almost saturated solutions of the material in 1,2,4-trichlorobenzene were applied on the basal plane of a freshly cleaved HOPG surface, and the physisorbed monolayers examined by STM without removing the solvent.

Among the three different macrocycles investigated, only compound **95d** could physisorb into highly ordered monolayers at the solution/HOPG interface. The STM current images are shown in Fig. 37, with the unit cells of the molecular arrangements and the models of the packing superimposed. The adsorbate unit cell possesses an oblique geometry: it amounts to a = 3.7 ± 0.2 nm, b = 3.5 ± 0.2 nm, α = 54 ± 3°. The result gained for cycle **95d** was interpreted by Samorí taking into account that the contrast in STM area images is ruled by both the degree of spatial overlap of the electronic states of the adsorbate with the ones of the substrate[157], and the difference between the energies of the molecular states of the absorbate and the Fermi level of the substrate. Thus, due to a larger energy difference, aliphatic chains on HOPG generally appear darker than moieties with π-electrons, provided

that the moieties are lying equally flat on the substrate.[158] An angular bright segment is visible and can be ascribed to the terphenyl unit. With a slightly less dark contrast, the unsubstituted terpyridine segments are located in the positions which are placed at the edges of the drawn unit cells. Their lower contrast, if compared to the terphenyl units, can be explained with both the different electronic structure of the moiety and with a different coupling with the electronic states of the substrate. This latter effect would be due to a diverse location along the z-axis of the conjugated orbitals with respect to the HOPG states. In particular, the fact that the contrast of the terpyridine segments is not elongated but rather appears as a spherical spot suggests that the two external pyridine rings are not planar with respect to both the central one and the basalt plane of the HOPG surface. The alkoxy and alkyl side chains are likely to be arranged according to a twofold symmetry, as observed for other "hairy discs".[159] In the present case, the high conformational mobility at the surface, which occurs on a time scale faster than the scanning frequency, did not allow us to resolve their structures. The overall molecular arrangement on the surface of graphite is loosely packed. This means that the gain in enthalpy upon absorption on HOPG is not very high.[157] This is most likely the reason for the low stability in time of the visualized 2-D crystals which indeed revealed high dynamics in the seconds time scale. Furthermore, since the imaging is extremely sensitive to tiny changes in the average tunneling current (also in the range of 1-5 pA), it was possible to record just a few images with such a molecular resolution.

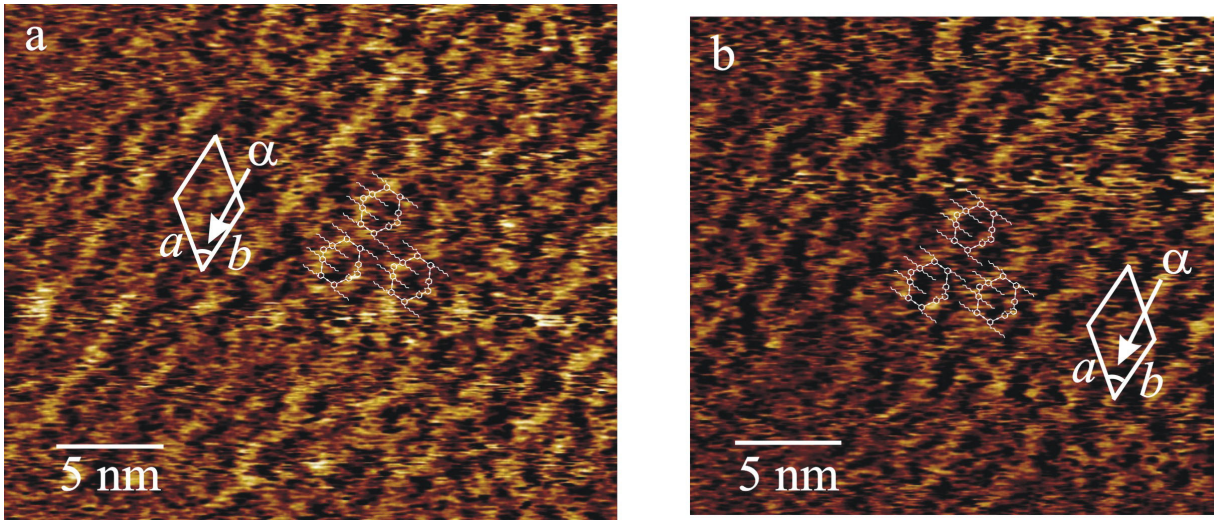

*Figure 37. STM current images of monolayers of **95d** on HOPG.*[155]

4.6.6 Liquid crystalline phases

Two types of discotic liquid-crystalline order are commonly observed. A discotic nematic (N_D) phase displays quasi long-range order of the director field (determined by unit vectors normal to the discs), but only liquid-like short-range positional order. In a discotic columnar phase (D), the molecules are arranged into columns, with short-range intercolumnar order and long range two-dimensional order (usually hexagonal, D_{hd}) of the columns. The disc-shaped molecules which form this latter structure most often have rigid, flat π-conjugated cores and flexible aliphatic substituents.[6] Shape-persistent macrocycles are especially interesting here, as they may be expected to form supramolecular tubes which can be used for transport processes.[160]

Moore examined his phenylacetylene macrocycles by optical microscopy, differential scanning calorimetry (DSC) and X-ray diffraction (XRD) and found evidence for different nematic or hexagonal-columnar liquid crystalline phases usually in temperature ranges of around 100-200°C.[6,161] The columnar order of the D phase was not destroyed when doped by small amounts of silver triflate. XRD analysis indicated that the ions were located inside the tubes. This result can be viewed as a first step towards the development of anisotropic liquid crystalline ionic conductors.

Höger observed a N_D phase for a macrocycle with a novel topology.[162] The rigid backbone formed the outer scaffold, while the flexible side chains were proposed to be located inside.

By DSC and optical microscopy, Henze could prove the occurrence of different liquid crystalline phases for his bipyridine macrocycles.[31] Attempts to elucidate the structure via XRD failed due to thermal decomposition of the material.

DSC measurements are based on the fact that supply or dissipation of heat at phase transitions does not lead to a change in temperature. Principally, transitions between the solid state, different mesoscopic phases and the isotopic melt can be detected; especially for mesoscopic phases, however, the energy involved is often very low. Measurements were done for cyclic compounds **95a**, **95d**, **110a** and **[110a]$_2$** (Fig. 38).[163] As effects observed during first heating can be ascribed to the "history" of the sample, measurements are performed at least twice. The results of the second heating are shown. The observed effects are too low to allow any interpretation of the curves for **[110a]$_2$** (not shown) and **110a**; only for **95a** and **95d**, glass-to-rubber transitions at ca 50 and 80 °C can be detected.

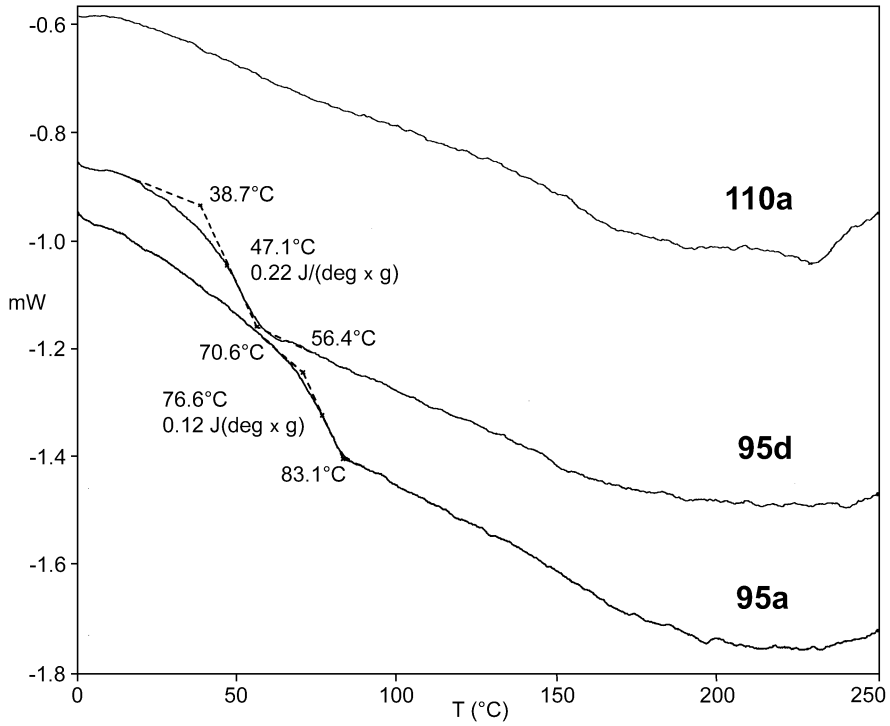

*Figure 38. DSC curves for macrocycles **95a**, **95d** and **110a**.*[163]

In the polarization microscope, textures were observed for **95a** between around 200°C and 150°C, which hint at liquid crystalline phases. Further measurements, however, are necessary here.

4.6.7 Higher cyclic fractions

A macrocyclization reaction between an A,A- and a B,B-functionalized precursor can yield different cyclic products. Not only the dimeric cycle from the reaction of one of each precursors, but also tetrameric, hexameric or even larger macrocycles can be expected. From a single A,A-functionalized precursor (as used, for example, in the Glaser reaction), cyclic systems from an uneven number of precursors can also form, i.e., trimeric or pentameric ones.

In the case of the shape-persistent macrocycles, the geometry of the precursors may lead to a selectivity in the cycles formed. The most remarkable example here is cycle **17** (Fig. 2, p. 10)[50] However, one should not overestimate the rigidity of shape-persistent macrocycles. From a Glaser coupling of (A,A-functionalized) precursors with two 60° kinks, Tobe did not isolate the expected hexagonal cyclic trimer but a mixture of the cyclic di- and tetramer.[142] Their geometry seemed unfavorable and he could give no explanation for this result. Some authors described the isolation and characterization of different cyclic oligomers from their coupling reactions, but, in most cases, where two half rings were coupled, higher oligomers were not analyzed.

In this work, the GPC traces of nearly all cyclizations showed peaks which may be assigned to cyclic tetra-, hexa- or even octamers (ref. Figs. 11, 12, 14, 16, 18, p. 49, 51, 55, 59, 62). The mass increments between a certain cyclic oligomer and the next are always considerably lower than calculated. This is due to the rigidity and geometry of the compounds, thus resulting in a relatively lower hydrodynamic volume compared to PS standard in GPC (ref. discussion on page 47). The tetrameric cycle, for example, would not be planar any more, but rather saddle-shaped (**T**, Fig. 39), thus coming nearer to the minimal spherical shape.

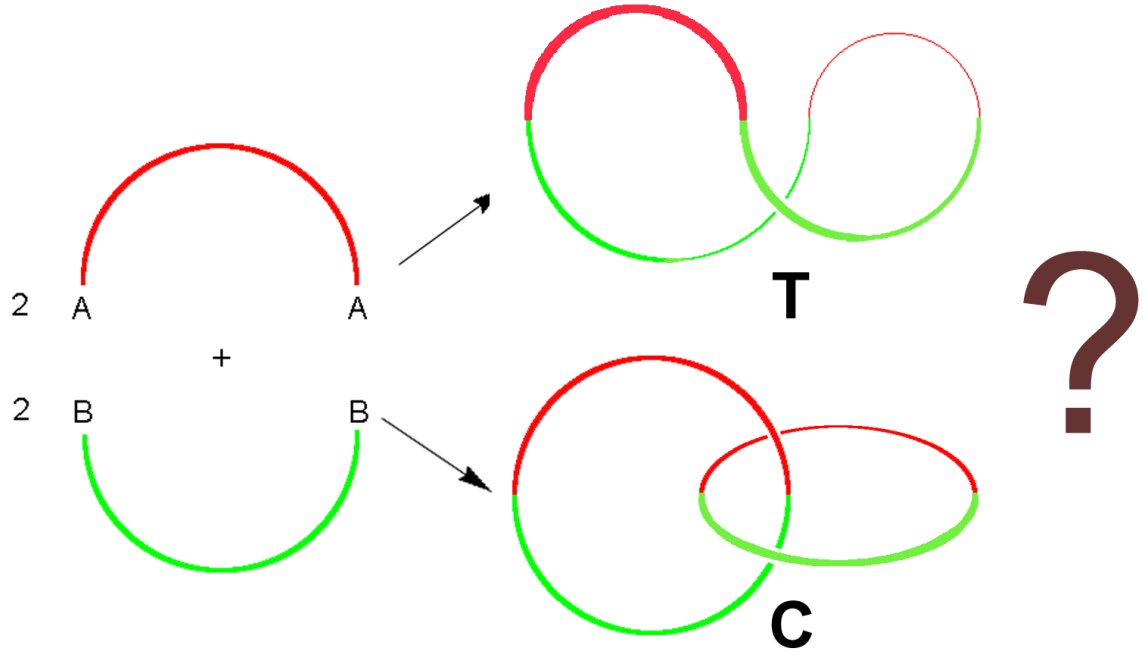

*Figure 39. Two possible cyclic tetramers can form from an A,A- and a B,B-functionalized shape-persistent half ring: A large tetrameric macrocycle (**T**), and a catenane of two dimeric macrocycles (**C**).*

For all macrocycles except **95d**, the fraction assigned as the double mass cycle was isolated from preparative GPC. The higher oligomers were not isolated. As far as the material could be characterized, the following features were found: (a) the mass (GPC) is roughly twice the mass of the cycle, as mentioned above; (b) the mass (MALDI) is exactly twice the mass of the expected cycle, and (c) in ^{1}H- and ^{13}C-NMR, their set of signals are practically identical. The signals, however, may be shifted (but the signals of the dimeric cycles show anyway strong chemical shifts in dependence on concentration).

All this can be seen as an evidence for the cyclic nature of these oligomers. However, this statement does exclusively apply to tetrameric macrocycles; two threaded dimeric

macrocycles, i.e., a catenane (**C**, Fig 39), can be expected to show the same characteristics in GPC, MS and NMR. For many smaller macrocycles, the formation of catenanes can be excluded as their interior is too small but this is surely not the case here. In literature, the problem is rarely discussed in publications dealing with shape-persistent macrocycles. Only Höger addressed this question when studying the yield in ring closure for two half rings covalently linked by a flexible template.[48] The fact that the length of the template, but not that of the half rings, influenced the cyclization yield, was interpreted as evidence that oligomerization rather than catenation is a dominant side reaction.

Problems to positively prove either a catenane or a macrocycle have also been encountered by Godt who approached this problem from a different viewpoint, i.e., aimed at catenanes.[164] The formation of a macrocycle could then be excluded on the basis of arguments dealing with observations in steps of synthesis, but not by direct interpretation of MS and NMR data. A positive proof for the catenane was later given by visualizing a 2-D array of these structures on HOPG with STM.[165] In many other works, the catenanes were unequivocally proven by X-ray crystallography.[166-168]

As catenane syntheses are generally based on a template approach,[169] the two threaded cycles in most cases interact in a certain way, i.e., by being coordinatively bound to the same metal center. Thus, the proof for catenanes rests upon the detection of these interactions. By NMR studies, for example, the proximity of certain protons can be shown,[166] and in one example, the absence of these observations has also led to the proof of a macrocycle instead of a catenane.[168]

Mass spectrometry has also been used to decide between catenanes and macrocycles. Under different MS conditions, cyclic β-ketolactones split into fragments by opening the cyclic backbone. In macrocyclic rings, at least two bonds are broken before fragments are observed, while in catenanes only a single bond is broken, thus leading to different fragmentation patterns.[170]

In summary, neither MS nor NMR can be expected to solve our problem in respect to these systems. For the dimeric macrocycles, in no case characteristic fragments from a dissociation of the cycles' backbone were observed in MS, and there were no characteristic interactions between the two macrocycles in a supposed catenane, which if observed in NMR could have proved or excluded catenane formation. Only imaging techniques like STM or X-ray diffraction on single crystals can be expected to lead to definite conclusions here. While attempts to grow single crystals analogously to those described earlier have so far failed, no STM measurements have been done yet.

MS spectra have been obtained for cyclic tetramers **[88]$_2$**, **[95a]$_2$** (Fig. 40), **[95b]$_2$** (FAB), **[95c]$_2$**, **[106]$_2$**, **[110b]$_2$** and **[111]$_2$** as well as for the trimer **[111]$_{1.5}$** (Fig. 41). For **[110b]$_2$** a dominant signal for $[M+Na]^+$ was observed besides a signal at higher m/z value, which could be assigned to a $[M+Cu]^+$ cluster. The copper ions may come from the CuI catalyst; it is, however, not clear why this effect is observed only in a few cases. For **[110a]$_2$** (Fig. 42) and **[110c]$_2$** the MALDI spectra showed a broad hill of peaks in the expected region; no single peak, however, could be assigned.

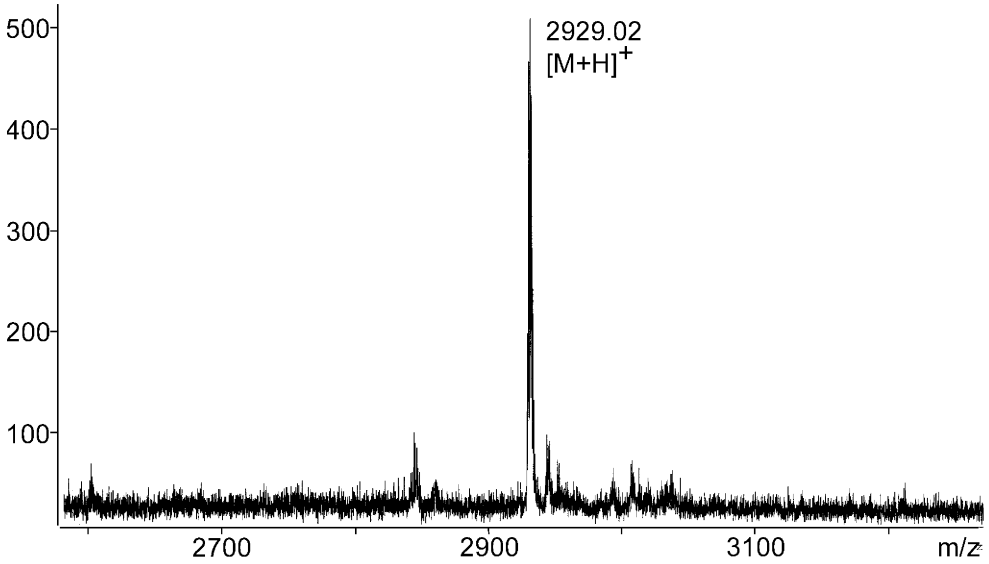

*Figure 40. MALDI-TOF MS spectrum (reflector mode, excerpt) of the macrocyclic tetramer **[95a]$_2$**.*

^{1}H-NMR spectra were recorded of the cyclic tetramers **[88]$_2$** (Fig. 43 middle), **[95a]$_2$**, **[95b]$_2$**, **[95c]$_2$**, **[106]$_2$**, **[110c]$_2$**, **[111]$_2$** and the trimer **[111]$_{1.5}$**. ^{13}C-NMR spectra were recorded of **[88]$_2$** (Fig. 43 bottom), **[95a]$_2$** (Fig. 44 bottom), **[95b]$_2$** and **[106]$_2$**. The ^{1}H-NMR spectra generally showed small traces of impurity; whether these are linear oligomers (which, however, were not detected in MS), is not clear. The best analyzed structure is **[88]$_2$**, whose spectra are shown and compared to the ^{1}H-NMR of **88** in Fig. 43. While **88** was only poorly soluble, and no 2-D spectra were recorded, **[88]$_2$** shows clean ^{1}H and ^{13}C NMR spectra, the signals of which could be assigned nearly completely (see discussion on the problems connected with NMR analysis of the macroycles here in Chapter 4.6.3) by HETCOR and COSY measurements. Especially in the aromatic region, the proton signals of **[88]$_2$** and **88** are shifted relative to each other. As previously mentioned, no conclusion can be drawn from this.

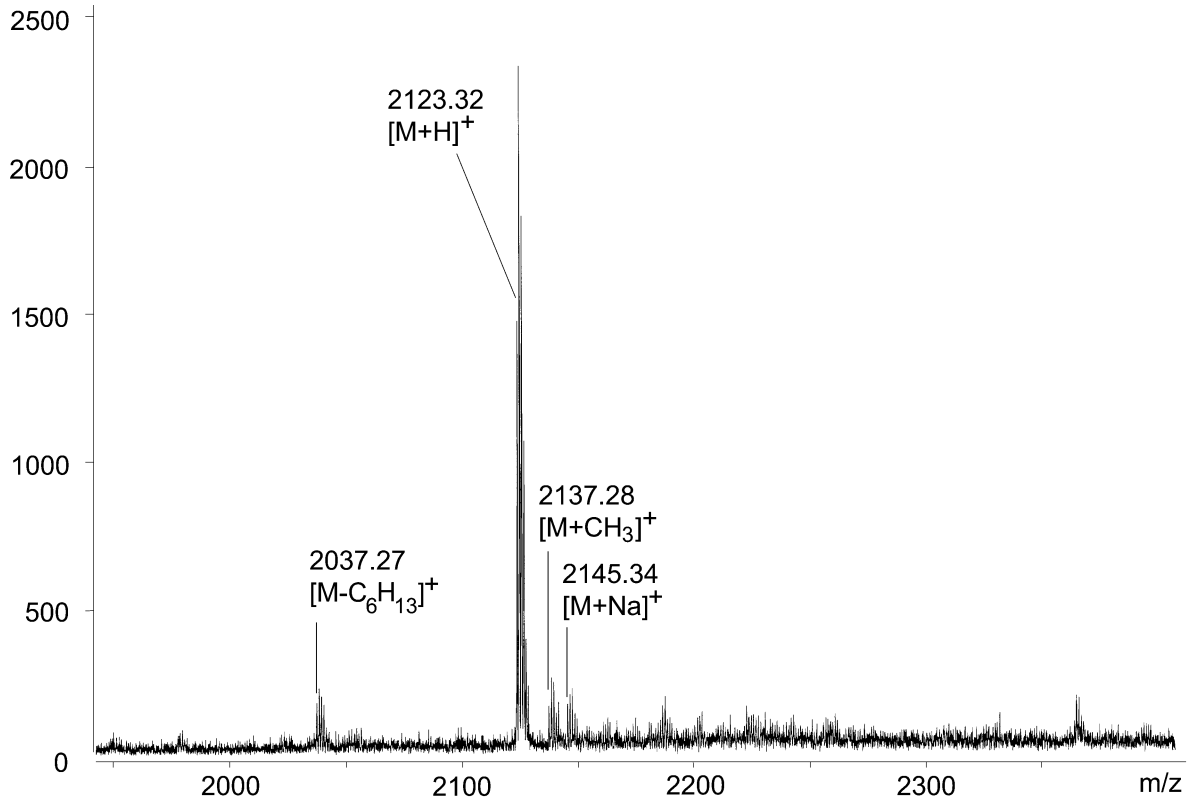

Figure 41. MALDI-TOF MS spectrum (reflector mode, excerpt) of macrocyclic trimer ***[111]****$_{1.5}$.*

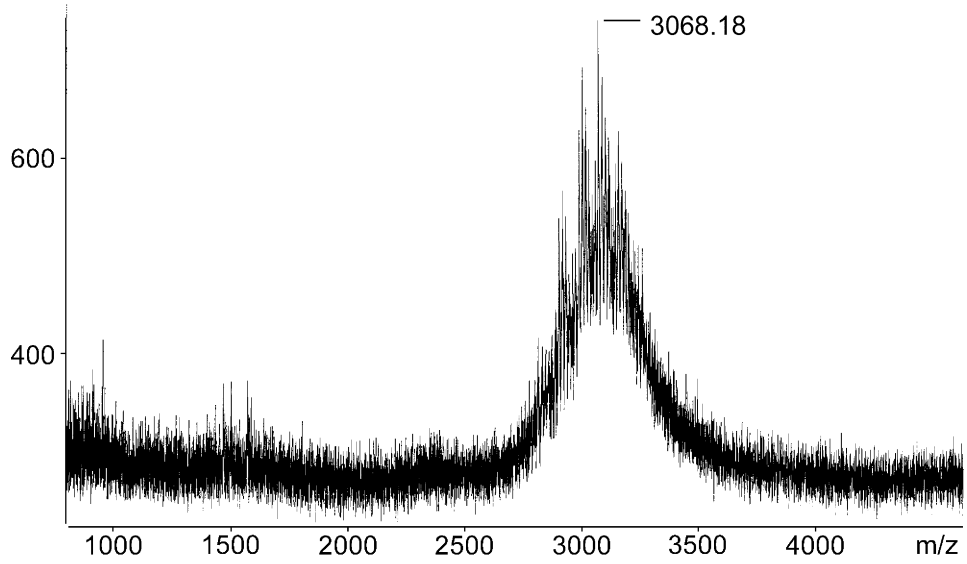

Figure 42. MALDI-TOF MS spectrum (linear mode, excerpt) of the supposed macrocyclic tetramer ***[110a]$_2$*** *(m/z = 3133.2).*

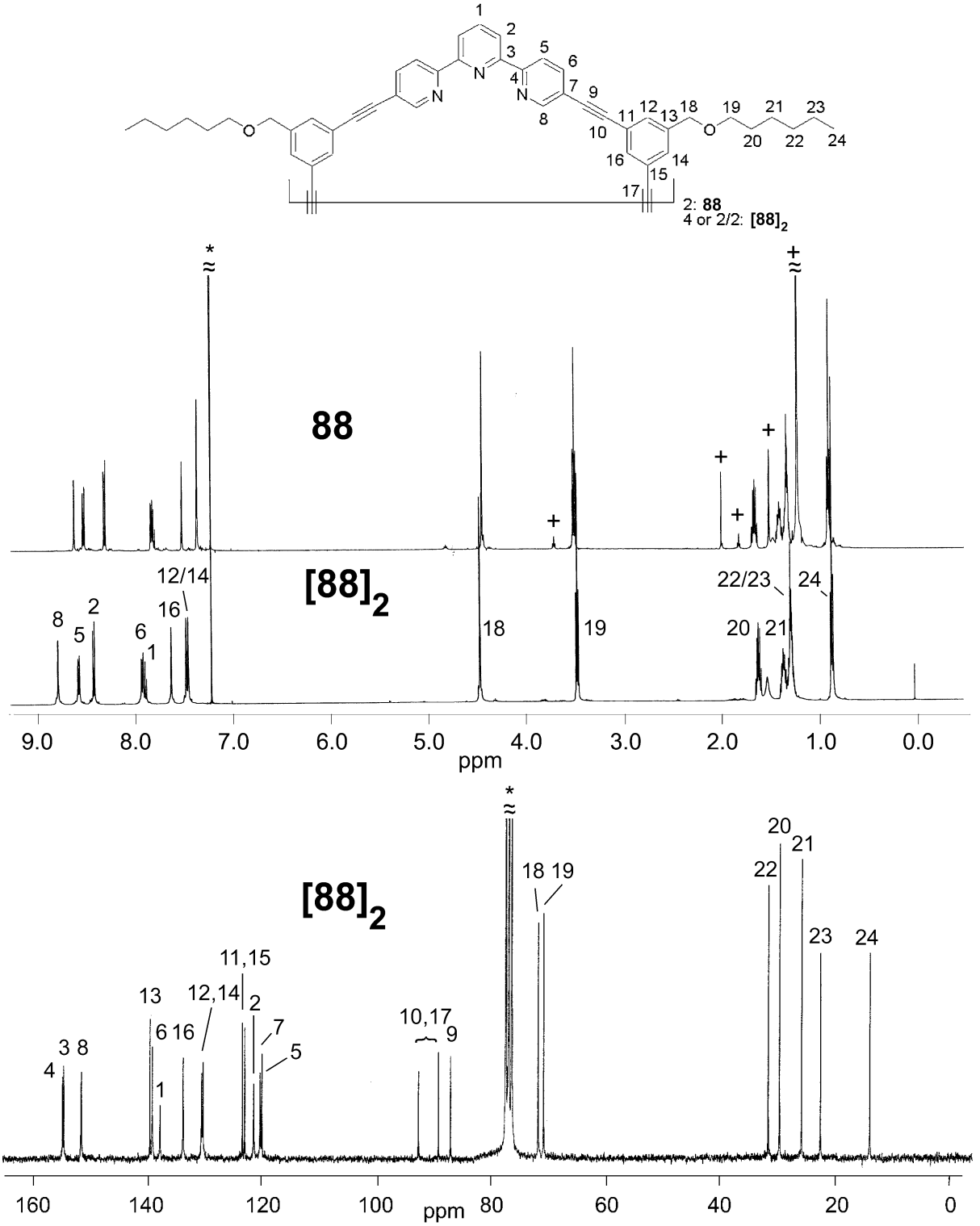

*Figure 43. ^{1}H-NMR spectra (500 MHz, $CDCl_3$) of compounds **88** and **[88]$_2$**, ^{13}C-NMR spectrum (125.8 MHz, $CDCl_3$) of **[88]$_2$**. * = $CDCl_3$, + = solvent impurities.*

A direct comparison between the ^{13}C spectra of the cyclic oligomers is given in the example of **95a** and **[95a]$_2$** (Fig. 44). One can see that the set of signals is nearly identical,

with some signals being shifted and more or less well separated. The signals for **95a** could be assigned by 2-D measurements (for details, see Exp. Part).

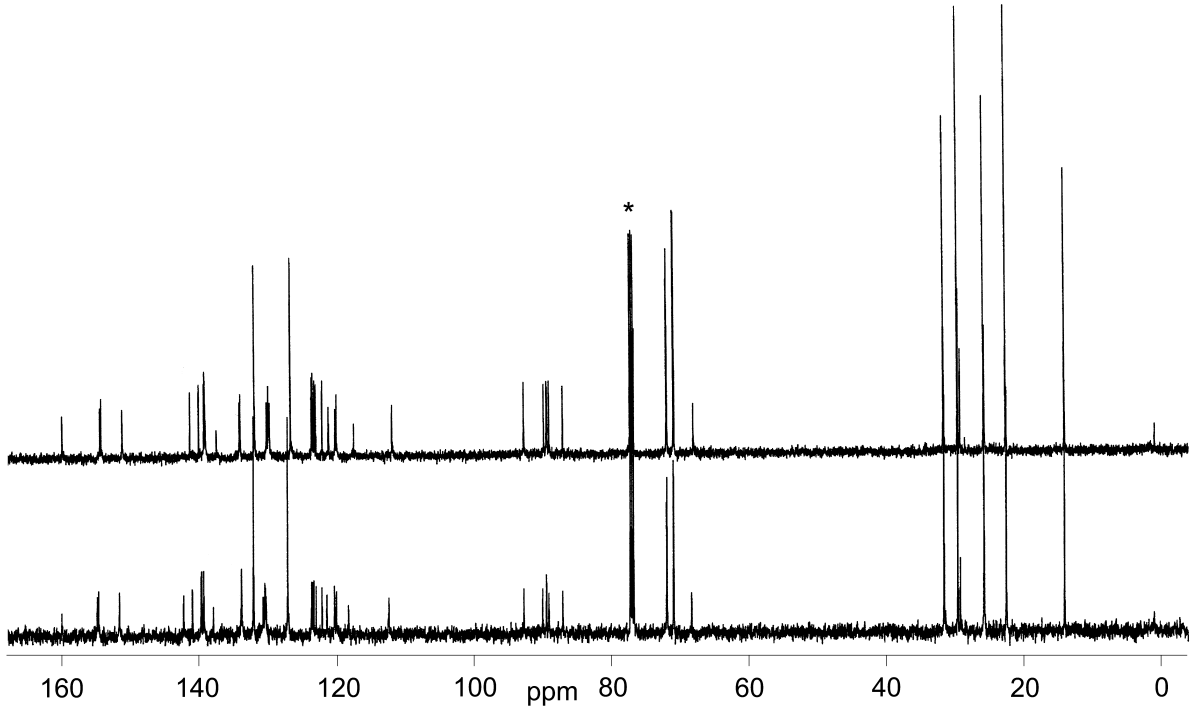

Figure 44. ^{13}*C-NMR spectrum (125.8 MHz,* $CDCl_3$*) of* ***95a*** *(top) and* ***[95a]*** $_2$ *(bottom).* ***** = $CDCl_3$.

The attempts to characterize the cyclic oligomers can be summarized as followed: The characterization is hampered by the same factors as those for the cyclic dimers, and especially for the oligomers **[110a]**$_2$**-[110c]**$_2$ with four terpyridine units, it was not even possible to get MALDI spectra. In no case, however, did the measurements hint at linear oligomers, but all recorded spectra backed the cyclic nature of the compounds.